In-plane dissipation as a possible synchronization mechanism for terahertz radiation from intrinsic Josephson junctions of layered superconductors

Shi-Zeng Lin[1,*] and Xiao Hu[2]

[1]*Theoretical Division, Los Alamos National Laboratory, Los Alamos, New Mexico 87545, USA*
[2]*International Center for Materials Nanoarchitectonics (WPI-MANA), National Institute for Materials Science, Tsukuba 305-0044, Japan*

Strong terahertz radiation from the mesa structure of a $Bi_2Sr_2CaCu_2O_{8+\delta}$ single crystal has been observed recently, where the mesa intrinsically forms a cavity. For a thick mesa of a large number of junctions, there are many cavity modes with different wave vectors along the c axis corresponding to almost the same bias voltages. The mechanism responsible for exciting the uniform mode which radiates coherent terahertz waves in experiments is unknown. In this paper, we show that the in-plane dissipation selects the uniform mode. For perturbations with nonzero wave numbers along the c axis, the in-plane dissipations are significantly enhanced, which prevents the excitation of corresponding cavity modes. Our analytical results are confirmed by numerical simulations.

I. INTRODUCTION

A layered cuprate superconductor, such as $Bi_2Sr_2CaCu_2O_{8+\delta}$ (BSCCO), intrinsically forms a stack of Josephson junctions.[1] Because of the large superconducting energy gap (60 meV), these build-in intrinsic Josephson junctions (IJJs) can support oscillations with frequencies in the terahertz (THz) band. IJJs are homogeneous and packed on a nanometer scale, much smaller than THz electromagnetic (EM) wavelength. If synchronized, they can radiate powerful THz EM waves. The radiation frequency is determined by the bias voltage according to the ac Josephson relation, thus in principle can be tuned continuously. The THz generator based on IJJs thus is promising to fill the THz gap.[2,3]

In 2007, coherent radiations from a mesa structure of BSCCO without external magnetic fields were detected experimentally.[4] The radiation frequency and voltage follow the ac Josephson relation, thus the radiation is due to the Josephson plasma oscillation in the mesa. The frequency f is determined by the lateral size L_x of mesa $f = c_0/(2L_x)$ with $c_0 = c/\sqrt{\epsilon_c}$ the Josephson plasma velocity where ϵ_c is the dielectric constant of BSCCO. The measured relation between L_x and f has revealed unambiguously that the mesa works as a cavity to synchronize plasma oscillations in different junctions. The cavity resonance mechanism has been confirmed by many independent experiments.[5–9]

The experiments raise several questions. First, in experiments a dc current is uniformly injected into the mesa. One thus expects the superconducting phase would oscillate homogeneously along the lateral directions, which, however, seemed to be hardly reconciled with the observed cavity modes. This question has been addressed in Refs. 10 and 11. They suggested that the superconducting phase develops π phase kinks near the cavity resonances. With the help of the π phase kink, the standing wave of electromagnetic fields can be stabilized and a large amount of energy is pumped into EM waves from the dc current.

Secondly, as the mesa intrinsically forms a three-dimensional (3D) cavity, cavity modes both along the c axis and ab plane can be excited. When the frequency of the plasma oscillation ω determined by the bias voltage

per junction is tuned to the cavity frequency $\omega'_c = \sqrt{(m_x\pi/L_x)^2 + (m_y\pi/L_y)^2}c_q$, the cavity mode (m_x, m_y) is excited,[12] where c_q depends on the wave vector $q = n\pi/(N+1)$ along the c axis with N the number of junctions and n an integer. For a large N, such as $N \approx 1000$ in experiments, there are many cavity modes with different q within a narrow window of bias voltage, and one would expect various modes should be excited when the voltage is swept. Nevertheless, for a given radiating sample, only the modes uniform along the c axis ($q = 0$) are observed upon sweeping current in experiment. The reason remains illusive.

Thirdly, understanding of possible cavity modes along the c axis is also important for getting stronger radiation from the mesa structure of BSCCO, which is still too weak for practical applications to date. The radiation power can be enhanced by using a thicker mesa with larger N, since the radiation power is proportional to N^2 in the superradiation region. One question is whether there exists a fundamental limiting factor besides the heating effect for N.

In this paper, we show analytically that in-plane dissipations prevent the excitation of nonuniform cavity modes along the c axis. For nonuniform perturbations with a large q, effective in-plane dissipations are greatly enhanced, and thus the perturbations quickly die out and no cavity mode is excited. For perturbations with a small q, in-plane dissipations are weak and vanish for $q = 0$. The weak dissipation along the c axis cannot damp them efficiently, and thus cavity modes with small q's are excited. For $N \approx 10^3$, only the cavity mode with $q = 0$ can be excited. While for large $N \approx 10^4$, modes with finite but small q vectors can also be excited and compete with mode $q = 0$. The analytical results are confirmed by direct numerical calculations. The mechanism to achieve synchronization by dissipation may be applied to other systems as well by preventing the excitation of the out-of-phase mode.

II. MODEL

We consider a stack of IJJs with lateral sizes $L_x \approx 80 \ \mu$m, $L_y \approx 300 \ \mu$m similar to those in experiments, see the inset of Fig. 1. Because $L_y \gg L_x$, we can assume that the
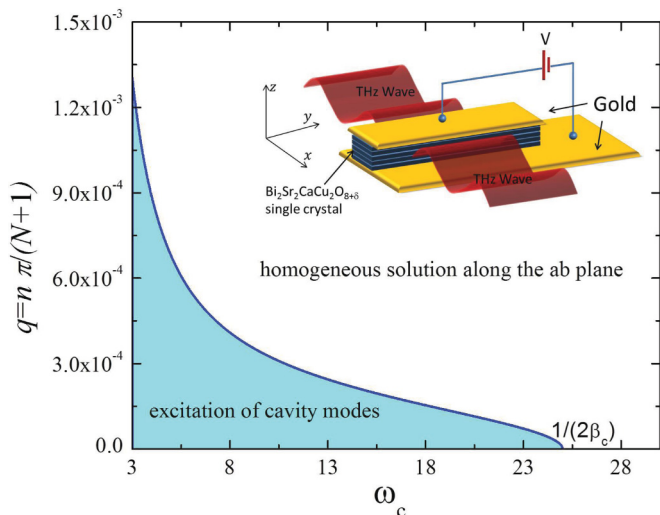
FIG. 1. (Color online) Stability diagram for the homogeneous solution along the *ab* plane. In the filled region, the homogeneous solution is unstable and the cavity mode (k_m, q) is excited. Inset is a schematic view of the setup for THz radiation.

superconducting phase is uniform along the *y* axis. The dynamics of the gauge invariant phase difference φ_l and magnetic field $B_{y,l}$ in the *l*th junction are described by[13–17]

$$\partial_t^2 \varphi_l + \beta_c \partial_t \varphi_l + \sin\varphi_l = \partial_x B_{y,l}, \quad (1)$$

$$[\zeta \Delta^{(2)} - (1 + \beta_{ab}\partial_t)]B_{y,l} + (1 + \beta_{ab}\partial_t)\partial_x \varphi_l = 0, \quad (2)$$

where $\Delta^{(2)} f_l \equiv f_{l+1} + f_{l-1} - 2f_l$ is the finite difference operator. $\zeta \approx 10^5$ is the inductive coupling, $\beta_c \approx 0.02$, and $\beta_{ab} \approx 0.2$ are the renormalized conductivity along the *c* axis and *ab* plane, respectively.[18] For BSCCO, it is well established that the in-plane conductivity σ_{ab} is much larger than the *c*-axis conductivity σ_c, from microwave,[19] infrared spectroscopy,[20] and transport[21] measurements. At temperature $T = 0$, $\sigma_{ab} \approx 4 \times 10^6 \ (\Omega \cdot m)^{-1}$ and $\sigma_c \approx 0.2 \ (\Omega \cdot m)^{-1}$. Both β_c and β_{ab} depend on frequency, but the dependence is weak in the interested frequency region.[22,23] In the following discussion we will neglect the frequency dependence. The generalization is straightforward as we are working in the frequency domain. The in-plane dissipation due to β_{ab} has been overlooked in many theoretical models.

Equations (1) and (2) are supplemented by the boundary conditions. When the phase oscillates uniformly along the *c* axis, strong radiation of EM waves occurs, which can be accounted for using the boundary condition[24,25]

$$B_y(\omega) = \mp \frac{E_z(\omega)}{Z(\omega)}, \quad Z = \frac{2}{\sqrt{\varepsilon_d} L_z \left[|k_\omega| - \frac{2i}{\pi} k_\omega \ln \frac{5.03}{|k_\omega| L_z} \right]}, \quad (3)$$

where $-$ (+) corresponds to the edge $x = L_x$ ($x = 0$), and $k_\omega = \omega \sqrt{\epsilon_d}$ with ϵ_d the dielectric constant of the dielectric medium outside the IJJs. For stacks with height $L_z \ll 100 \ \mu$m, $Z \gg 1$. For nonuniform oscillations along the *c* axis, the radiation is weak and we can use the nonradiating boundary condition $B_{y,l} = \pm I_{ext} L_x/2$ with I_{ext} the bias current. We assume that the IJJs stack is sandwiched by two good conductors, such that the tangential current inside the conductor is zero. We use the boundary condition $B_{y,l=1} = B_{y,l=0}$ and similarly

for $l = N$, which corresponds to $\partial_z B_y(z) = 0$ in the continuum limit.

III. INSTABILITY OF THE HOMOGENEOUS SOLUTION

In experiments, one first ramps up the bias current and when current exceeds the critical one, the IJJs switch into the resistive state. One then reduces the current to the target value where radiation is observed. In the resistive state with the current close to the critical one, the phase φ_l oscillates homogeneous along the *x* direction. The phases may be either uniform along the *c* axis or different in different junctions. Here we show that the solution with φ_l homogeneous along the *x* direction is unstable when the bias current is reduced and that only the cavity modes with a long wavelength $q \ll 1$ along the *c* axis can be excited.

For the uniform solution along the *c* axis $\varphi_l = \varphi_0$, the solution to Eqs. (1) and (2) in the THz frequency region $\omega \gg 1$ can be written as $\varphi_0 = \omega t + g(x) \exp(i\omega t)$ with

$$g(x) = \frac{1}{-\omega^2 + i\beta_c \omega} \left[i - \frac{\cos\left[(x - L_x/2)\omega\right]}{Z \sin(L_x \omega/2) - i \cos(L_x \omega/2)} \right]. \quad (4)$$

The first term in the square bracket of Eq. (4) is due to plasma oscillation and the second term is due to radiation. The frequency ω can be tuned by the bias current I_{ext} (or voltage).

To reveal the instability of the homogeneous solution, we add small perturbations to the uniform solution $\varphi_l = \varphi_0 + \theta_l$, $B_{y,l} = B_0 + \tilde{B}_{y,l}$ with $B_0 = \partial_x \varphi_0$, $\theta_l \ll 1$ and $\tilde{B}_{y,l} \ll 1$. Since the perturbations are nonuniform along the *c* axis, the radiation contribution can be neglected, thus we can use the nonradiating boundary condition, $\partial_x \theta_l = 0$ and $\tilde{B}_{y,l} = 0$. The solution for θ_l and $\tilde{B}_{y,l}$ can be written as

$$\theta_l(x,t) = \sum_{m,q,p} \cos(ql) \cos(k_m x) a_p(m,q) \exp[i(p\omega - \Omega)t] \quad (5)$$

$$\tilde{B}_{y,l}(x,t) = \sum_{m,q,p} \cos(ql) \sin(k_m x) b_p(m,q) \exp[i(p\omega - \Omega)t], \quad (6)$$

with $k_m = m\pi/L_x$, $q = n\pi/(N+1)$ and p an integer. The perturbations with frequency Ω couple with the nonlinear Josephson current $\sin\varphi_l$ and induce frequency harmonics $p\omega - \Omega$.[26] From Eq. (2), we have $b_p = -c_q^2 k_m a_p$ with the plasma velocity $c_q(\omega) = [1 + 2\zeta(1 - \cos q)/(1 + \beta_{ab}i\omega)]^{-1/2}$. Substituting Eqs. (5) and (6) into Eqs. (1) and (2), and comparing each frequency component, we obtain an equation for perturbations

$$[\omega_m^2(\omega_p) - \omega_p^2 + i\omega_p \beta_c]a_p + \frac{a_{p-1} + a_{p+1}}{2}$$
$$- \frac{A_{p-2} - A_p}{2i} = 0,$$

where $\omega_m^2 = c_q^2 k_m^2$, $\omega_p = p\omega - \Omega$, and $A_p = \frac{2}{L_x} \int_0^{L_x} dx$ $g(x)\theta_p(x)\cos(k_m x)$. Because of the in-plane damping β_{ab}, ω_m^2 is a complex number. We can split ω_m^2 into real and imaginary

parts $\omega_m^2(\omega) = \Omega_m^2(\omega) + i\mathcal{B}_{ab}(\omega)\omega$, with

$$\Omega_m^2(\omega) = \frac{1 + 2\zeta(1-\cos q) + \beta_{ab}^2\omega^2}{[1+2\zeta(1-\cos q)]^2 + \beta_{ab}^2\omega^2}k_m^2, \quad (7)$$

$$\mathcal{B}_{ab}(\omega) = \frac{2\zeta(1-\cos q)\beta_{ab}}{[1+2\zeta(1-\cos q)]^2 + \beta_{ab}^2\omega^2}k_m^2. \quad (8)$$

$\Omega_m(\omega)$ is the cavity resonance frequency for the mode (k_m, q). For the nonuniform perturbations along the c axis $q > 0$, the effective in-plane damping is enhanced according to $\mathcal{B}_{ab}$. It is this enhanced in-plane dissipation that prevents the excitation of a nonuniform cavity mode along the c axis with a large q as revealed later.

In the region of $\omega_m \gg 1$ and $\beta_c \ll 1$, we have $|\Omega_m^2 - \omega_{p=0}^2| \ll 1$. Thus the dominant wave vector of $\theta_p(x)$ is k_m. The dominant wave vector for $g(x)$ is $k_x = 0$ because the radiation contribution is small. Then we can approximate $\theta_p(x)g(x)$ by $\bar{g}\theta_p(k_m)\cos(k_m x)$ with $\bar{g}$ the spatial average of $g(x)$, because other modes are negligibly small. Neglecting the small dissipation contribution β_c in $\bar{g}$, we have

$$\frac{\bar{g}}{2i} = \frac{1}{-2\omega^2} + \frac{1}{L_x\omega^3[\cot(L_x\omega/2) + Zi]} = \frac{1}{-2\omega^2} + R_r + iR_i,$$

where R_r is the real part of the radiation contribution and R_i is the imaginary part. We then have $A_p = \bar{g}a_p$. The equation for perturbations then can be written as

$$\left[\Omega_m^2 - \omega_p^2 + R_r - \frac{1}{2\omega^2}\right]a_p + i[\omega_p(\beta_c + \mathcal{B}_{ab}) + R_i]a_p$$
$$+ \frac{1}{2}(a_{p-1} + a_{p+1}) + \frac{1}{2\omega^2}a_{p-2} - R_r a_{p-2} - iR_i a_{p-2} = 0. \quad (9)$$

The radiation shifts the resonance frequency by R_r and also the contribution to the damping through R_i. Both R_r and R_i have the order $1/\omega^2 \ll 1$ for $L_x \sim 1$. The resonant frequency for perturbations with a wave vector (k_m, q) is $\Omega = \omega_c$ with ω_c given by $\omega_c^2 = \Omega_m^2(\omega_c) + R_r(\omega) - \frac{1}{2\omega^2}$. ω_c is also the cavity frequency for the cavity mode (k_m, q).

We then show that the parametric instability develops at a voltage when $\omega = 2\omega_c + \delta$ with $\delta \ll 1$. As $\Omega \approx \Omega_m \approx \omega_c$, the dominant frequency components are $p = 0$ and 1. The other frequency harmonics ($p > 1$ or $p < 0$) are small because their amplitude is of order $([(2p-1)^2 - 1]\Omega_m^2)^{-1}a_{0,1} \ll a_{0,1}$ thus can be neglected. Then Eq. (9) can be written as

$$[-2\omega_c\Omega_\delta + i(-\omega_c(\beta_c + \mathcal{B}_{ab}) + R_i)]a_0 + a_1/2 = 0, \quad (10)$$

$$[-2\omega_c(\delta - \Omega_\delta) + i(\omega_c(\beta_c + \mathcal{B}_{ab}) + R_i)]a_1 + a_0/2 = 0, \quad (11)$$

with $\Omega = \Omega_\delta + \omega_c$ and $\Omega_\delta \ll 1$. The spectrum of the perturbations Ω is given by equating the determinant of the coefficients matrix in Eqs. (10) and (11) to zero, which yields

$$\Omega_\delta = \left(-\frac{i\mathcal{B}_{ab}}{2} - \frac{i\beta_c}{2} + \frac{\delta}{2}\right)$$
$$\pm \left(\frac{i}{4\omega_c} - \frac{i}{2}\omega_c\delta^2 - \delta R_i + \frac{i}{2\omega_c}R_i^2\right).$$

The homogeneous solution along the x direction is unstable when $\text{Im}[\Omega_\delta] > 0$, which gives

$$\delta^2 < -\frac{(\mathcal{B}_{ab}(\omega_c) + \beta_c)}{\omega_c} + \frac{1}{2\omega_c^2} + \frac{1}{\omega_c^2}R_i^2. \quad (12)$$

From this expression, it becomes clear that the radiation tends to destabilize the homogeneous solution, albeit with a small impact $R_i \sim 1/\omega^2 \ll 1$. More importantly, both the effective in-plane dissipation $\mathcal{B}_{ab}$ and dissipation along the c axis β_c tend to stabilize the solution homogeneous along the x axis. For long wavelength perturbations along the c axis, $\zeta q^2 \ll 1$, the dissipation is weak $\mathcal{B}_{ab}(\omega_c) + \beta_c < 1/(2\omega_c)$ thus the cavity mode (k_m, q) can be excited. By using Eqs. (7), (8), and (12), the condition for the excitation of the mode (k_m, q) for $\beta_{ab} > 0$ is

$$q^2 < -\frac{1}{\zeta}\left(\beta_c - \frac{1}{2\omega_c}\right)(1 + \beta_{ab}^2\omega_c^2)\left(\omega_c^2\beta_{ab} + \beta_c - \frac{1}{2\omega_c}\right)^{-1}. \quad (13)$$

The stability diagram is presented in Fig. 1 with the given parameters. Only the cavity mode with long wavelength along the c axis can be excited. As $q = n\pi/(N+1)$, for $N \approx 10^3$ used in experiments, only the uniform cavity $n = 0$ can be excited. For a larger $N > 10^4$, modes with finite but small n can also be excited.

For the solution that is homogeneous along the x axis but nonuniform along the c axis, the radiation contribution can be neglected and the phase oscillates according to $\varphi_l = \phi_l + \omega t + i/(-\omega^2 + i\beta\omega)$, where ϕ_l accounts for the phase shifts in different junctions and is randomly distributed. The stability analysis is the same as the case of uniform solution, but now there is no radiation contribution $R_r = R_i = 0$. The stability diagram is the same as that in Fig. 1 because the radiation contribution is small for $L_x \approx 80\,\mu$m used in experiments.

For a small crystal proposed in Ref. 25, $L_x \approx 4\,\mu$m, $\omega_c \approx 150$. The cavity modes cannot be excited for such a high frequency according to Eq. (13). The homogeneous solution along the lateral directions is thus stable. In the single junction limit $N = 1$, the parametric instability leads to the excitation of solitons, which manifests as the zero-field current step in IV characteristics.[27]

For nonuniform perturbations along the c axis, the in-plane current $J_{x,l}$ is induced according to the Ampere's law $4\pi J_{x,l}/c = -(B_{y,l+1} - B_{y,l})/s$ where we have neglected the displacement current.[14] $J_{x,l}$ has contribution from the normal current and supercurrent $J_{x,l} = \sigma_{ab}\frac{\Phi_0}{2\pi c}\partial_t\mathcal{P}_l + \frac{c\Phi_0}{8\pi^2\lambda_{ab}^2}\mathcal{P}_l$ where $\mathcal{P}_l = \partial_x\Theta_l - 2\pi A_x/\Phi_0$ is the in-plane superconducting momentum with superconducting phase Θ_l and vector potential A_x. The in-plane dissipation in units of $\frac{\omega_J}{4\pi}(\frac{\Phi_0}{2\pi\lambda_c s})^2$ is

$$P_{ab}(k_m, q, \omega) = \frac{2\sin^2(q/2)\beta_{ab}\omega^2}{(\beta_{ab}\omega)^2 + 1}|c_q^4|k_m^2|a_p(k_m, q)|^2, \quad (14)$$

which is much larger than the dissipation along the c axis $P_c(k_m, q, \omega) = \frac{1}{2}\omega^2\beta_c|a_p(k_m, q)|^2$ for q's when $\sin^2(q/2) > [(\beta_{ab}\omega)^2 + 1]/[4\beta_{ab}|c_q^4|k_m^2]$. Thus the nonuniform perturbations with a large q quickly die out due to the strong in-plane dissipation P_{ab}, while for perturbations with $q \ll 1$ the in-plane dissipation is weak or absent, and the perturbations lead to the excitation of the cavity mode with a small q.
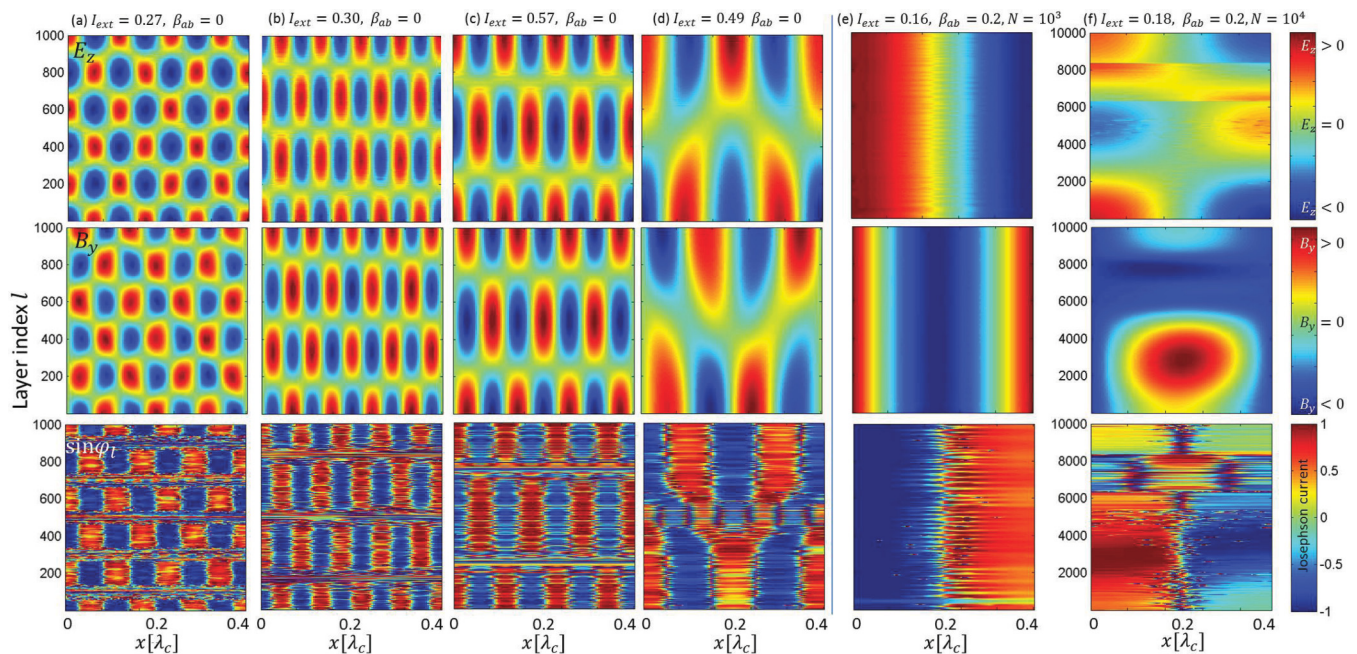
FIG. 2. (Color online) Snapshots of the electric field (first row), magnetic field (second row), and Josephson current $\sin(\varphi_l)$ (third row) without the in-plane dissipation $\beta_{ab} = 0$ [(a)–(d)] and with the in-plane dissipation $\beta_{ab} = 0.2$ [(e)–(f)]. When $\beta_{ab} = 0$, various cavity modes $(m,n) = (7,5)$ in (a), $(m,n) = (9,3)$ in (b), $(m,n) = (7,2)$ in (c) and $(m,n) = (4,1)$ in (d) are excited when the bias current is swept. For $\beta_{ab} = 0.2$, only the modes with $n = 0$, $[(m,n) = (1,0)$ in (e), other cavity modes with $m > 1$ are not shown here] are excited for $N = 10^3$. For $N = 10^4$, irregular patterns of the EM fields are excited even with the in-plane dissipation $\beta_{ab} = 0.2$. The supercurrent forms blocks with alternating sign between neighboring blocks indicating $\pm\pi$ phase jumps at the interface of each block. We use $L_x = 0.4\lambda_c$, $\zeta = 7.1 \times 10^4$ in simulations.

IV. NUMERICAL SIMULATION

We also perform numerical simulations by solving Eqs. (1) and (2) with the nonradiation boundary condition $B_{y,l} = \pm I_{ext}L_x/2$ to check the above analytical results. For numerical details, see Appendix A. Let us first present the results without in-plane dissipation $\beta_{ab} = 0$ as shown in Figs. 2(a)–2(d). Upon sweeping the current, various cavity modes both along the x axis and c axis are excited for $N = 10^3$. It is difficult to excite the uniform mode $q = 0$ due to the existence of other competing cavity modes in the crystal with this large N at a given voltage. Interestingly, when we turn on the in-plane dissipation by putting $\beta_{ab} = 0.2$, only the cavity modes uniform along the c axis can be excited when the current is swept as shown in Fig. 2(e), consistent with the above analytical results. The corresponding IV characteristics are shown in Fig. 3. At the cavity resonances, a large amount of energy is pumped into the plasma oscillation and current steps are induced, and the radiation power is enhanced.

For $N \lesssim 4000$ in simulations, only the uniform mode can be excited due to the in-plane dissipation, consistent with the results in Fig. 1. For an even larger number of IJJs, such as $N = 10^4$, irregular patterns of EM fields are developed in simulations for the adopted parameters, see Fig. 2(f). It is consistent with the analytic result summarized in Fig. 1 where cavity modes with $n = 0,1,2$ can be excited. Other mechanisms to synchronize all junctions are needed in order to achieve strong radiation for thick mesas. Here, we note that for small values of $N < 100$, the voltage corresponding to various cavity modes is discrete because c_q is well separated

for different values of n, thus one can select the cavity modes simply by tuning the voltage.

For $\beta_{ab} = 1.0$, we found numerically that the uniform plasma oscillation with $q = 0$ becomes stable again for $N = 10^4$. This suggests that stronger in-plane dissipation is important to achieve uniform plasma oscillation. β_{ab} increases with temperature, while on the other hand thermal fluctuations tend to destroy the uniform oscillation. Therefore the synchronization is optimal at some intermediate temperatures.

One peculiar feature in Fig. 2 is that the supercurrent forms blocks in space, where the current changes sign between
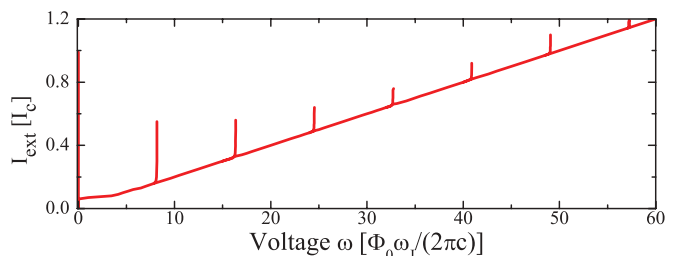
FIG. 3. (Color online) IV curve obtained with $\beta_{ab} = 0.2$ and $N = 10^3$. Other parameters are the same as those in Fig. 2. The radiation power is estimated using $S_r = |E_{ac}^2|/(2|Z|)$ and $\epsilon_d = 1$ where E_{ac} is the averaged ac electric field at edges.[28] The maximal power at the first cavity mode $m = 1$ is about 2800 W/cm^2. The experimental measured IV deviates significantly from the theoretical one in the high bias region due to the strong self-heating effect.

neighboring blocks, or equivalently at nodes of the oscillating electric field. This means that there is a $\pm\pi$ phase jump or $\pm\pi$ phase kink at the interface of blocks. The phase kinks stack along the c axis with alternating signs, such as $(\ldots,1,-1,1,-1,\ldots)\pi$. The state with the phase kink with $q=0$ was first suggested in Refs. 10 and 11 as a possible mechanism for strong THz radiation observed in experiments. A characterization of the kink state with a general q is presented in Appendix B.

V. DISCUSSIONS

One should also check the stability of the excited cavity modes. This has already been done in Refs. 28–30 and found that the kink states associated with cavity modes with $q=0$ are stable for a small N, which is also confirmed by the results in Fig. 2. For a large N, it was shown in Ref. 30 that long wavelength instability develops and the kink states with uniform plasma oscillation $q=0$ become unstable. This is consistent with the results in Fig. 2(f).

When a strong magnetic field is applied parallel to the ab plane, the Josephson vortices (JVs) are induced. The JVs favor the triangular lattice in the low velocity region due to the strong intervortex repulsion in a long IJJs stack.[31] As shown in Appendix C, our simulations show that the in-plane dissipation mechanism becomes insufficient to achieve the rectangular JVs lattice and in-phase plasma oscillation, consistent with the analytical results in Ref. 17. A new mechanism for synchronization is needed in this case.

APPENDIX A: NUMERICAL METHOD

Here we present the numerical method to solve Eqs. (1) and (2). The model is discrete inherently along the c axis, and we only need to discretize along the x axis. The phase φ is defined at nodes (j,l), and the magnetic field B_y is defined at nodes $(j+1/2,l)$ with integer j and l, see Fig. 4. The grid size along x is dx, and the time step is dt. Equation (1) then

becomes

$$\frac{\varphi_{l,j}^{m+1}+\varphi_{l,j}^{m-1}-2\varphi_{l,j}^{m}}{dt^2}+\beta_c\frac{\varphi_{l,j}^{m+1}-\varphi_{l,j}^{m-1}}{2dt}$$
$$+\sin\varphi_{l,j}^{m}=\frac{B_{l,j+1/2}^{m}-B_{l,j-1/2}^{m}}{dx}. \tag{A1}$$

We know φ and B_y at the mth time step, and we can obtain φ at the $(m+1)$th step directly from Eq. (A1). We use an implicit method to discretize Eq. (2). After some simple manipulations, we have

$$\frac{\varphi_{l,j+1}^{m+1}-\varphi_{l,j-1}^{m+1}+\varphi_{l,j+1}^{m}-\varphi_{l,j-1}^{m}}{2dx}$$
$$+\beta_{ab}\frac{\left(\varphi_{l,j+1}^{m+1}-\varphi_{l,j-1}^{m+1}\right)-\left(\varphi_{l,j+1}^{m}-\varphi_{l,j-1}^{m}\right)}{dt\,dx}$$
$$+\beta_{ab}\frac{B_{l,j+1/2}^{m}}{dt}-(1-\zeta\,\Delta^{(2)})\frac{B_{l,j+1/2}^{m}}{2}$$
$$=(1-\zeta\,\Delta^{(2)})\frac{B_{l,j+1/2}^{m+1}}{2}+\beta_{ab}\frac{B_{l,j+1/2}^{m+1}}{dt}. \tag{A2}$$

Equation (A2) can be written as a matrix equation. Inverting the matrix at the right-hand side of Eq. (A2) using $\varphi_{l,j}^{m+1}$ obtained from Eq. (A1), we then obtain $B_{l,j+1/2}^{m+1}$. The electric field is given by $E_{l,j}^{m}=(\varphi_{l,j}^{m+1}-\varphi_{l,j}^{m-1})/(2dt)$.

APPENDIX B: CHARACTERIZATION OF THE KINK STATE WITH A GENERAL q

In the kink state, φ_l can be written as

$$\varphi_l=\omega t+\varphi_{s,l}(x)-i\sum_{m,q}A_{m,q}\cos(k_m x)\cos(ql)\exp(i\omega t),$$
$$\tag{B1}$$

where the rotating phase at the right-hand side (rhs) of Eq. (B1) is due to the voltage, the second term at the rhs is the static phase kink, and the last term at the rhs is the cavity mode both along the c axis and x axis. For stacks with a large N, there are many cavity modes (m,q) corresponding to a same frequency ω, thus a summation over all modes are needed.[28] The magnetic field is

$$B_l=B_{s,l}(x)-i\sum_{m,q}C_{m,q}\sin(k_m x)\cos(ql)\exp(i\omega t), \tag{B2}$$

where $B_{s,l}$ is the static magnetic field due to the phase kink. We have neglected the frequency harmonics in Eqs. (B1) and (B2), which is valid when $A_{m,q}<1$. From Eq. (2) we obtain $C_{m,q}=-A_{m,q}k_m c_q^2$ and $[1-\zeta\Delta^{(2)}]B_{s,l}(x)=\partial_x\varphi_{s,l}(x)$. Substituting Eqs. (B1) and (B2) into Eq. (1), we obtain a closed equation for φ_l. For the frequency component ω, we have

$$\left[ik_m^2 c_q^2-(\beta_c\omega+i\omega^2)\right]A_{m,q}\cos(k_m x)\cos(ql)=-ie^{i\varphi_{s,l}}. \tag{B3}$$

Projecting $\exp(i\varphi_s)$ into the cavity mode (m,q), we obtain the amplitude of the plasma oscillation

$$A_{m,q}=\frac{-iF_{m,q}}{ik_m^2 c_q^2-(\beta_c\omega+i\omega^2)}, \tag{B4}$$

FIG. 4. (Color online) Schematic view of the numerical grids.

with the coupling between the cavity mode and phase kink

$$F_{m,q} = \frac{\alpha}{NL_x} \sum_{l=0}^{N} \int \exp(i\varphi_{s,l}) \cos(k_m x) \cos(ql) \, dx, \quad \text{(B5)}$$

where $\alpha = 2$ for $q = 0$ and $\alpha = 4$ for $q > 0$. When the voltage is tuned close to the cavity resonance, the amplitude of plasma oscillation is enhanced. The linewidth of the resonance is determined by β_{ab} and β_c. The *IV* characteristics are given by $I_{ext} = \beta_c \omega + \langle \sin(\varphi_l) \rangle_{x,l,t}$ where $\langle \cdots \rangle_{x,l,t}$ denotes average over space and time. We then obtain

$$I_{ext} = \beta_c \omega + \text{Re} \left[\sum_{m,q} \frac{|F_{m,q}|^2/(2\alpha)}{i k_m^2 c_q^2 - (\beta_c \omega + i\omega^2)} \right]. \quad \text{(B6)}$$

Now let us consider the static component

$$\partial_x^2 \varphi_s(x,z) = \frac{i\zeta}{2} \Delta^{(2)} \sum_{m,q} \left[A_{m,q} \cos(k_m x) \cos(ql) e^{-i\varphi_{s,l}} \right]. \quad \text{(B7)}$$

The solution of $\varphi_{s,l}$ depends on the spatial profile of the plasma oscillation. To present the analytical results, we consider a case where the plasma profile has well-defined nodes as shown in Figs. 2(a)–2(d), where we may approximate the spatial profile by a dominant mode $A \cos(k_1 x) \cos(ql)$. Without loss of generality, we have taken the $m = 1$ mode. The variation of $\varphi_{s,l}$ along the c axis is $\varphi_{s,l} = (-1)^l \varphi_{s0}$ except for the node region of the plasma oscillation, which is much faster than the plasma mode q. We may approximate Eq. (B7) as

$$\partial_x^2 \varphi_{s0} = 2\zeta \, \text{Re}[A] \cos(k_1 x) \cos(ql) \sin(\varphi_{s0}). \quad \text{(B8)}$$

Equation (B8) is invariant under the transformation $x \leftarrow L_x - x$ and $\varphi_{s0} \leftarrow \pi - \varphi_{s0}$, which gives the static π phase kink along the x axis at the nodes of oscillating electric field when $\cos(k_1 x) = 0$. The width of the kink is $\lambda_k = 1/\sqrt{2\zeta \text{Re}[A] |\cos(ql)|}$, which is small $\lambda_k \ll 1$ except for the node region of $\cos(ql) \approx 0$. The kink in the lth junction can be

excited only when $\lambda_k \ll L_x$. Near the nodes of the oscillating E_z or B_y along the c axis where $\cos(ql) \approx 0$, λ_k may be comparable to L_x, thus no kink exists in the node region, consistent with results in Fig. 2. When $\cos(ql)$ changes sign, φ_{s0} acquires a π shift, because Eq. (B8) is invariant when $\cos(ql) \leftarrow -\cos(ql)$ and $\varphi_{s0} \leftarrow \pi + \varphi_{s0}$. Thus there are $\pm\pi$ phase jumps at the nodes of oscillating electric fields both along the c and x axis.

APPENDIX C: EFFECT OF THE IN-PLANE DISSIPATION ON THE DYNAMICS OF JOSEPHSON VORTICES

When a strong magnetic field is applied perpendicular to the c axis of a BSCCO single crystal, the Josephson vortices are induced and form the triangular lattice. Driving by the Lorentz force induced by a transport current, the Josephson vortices move and excite Josephson plasma. The motion of the Josephson vortex lattice provides an alternative routine to achieve a strong THz radiation.[32] Due to the strong intervortex repulsion, the Josephson vortices favor the triangular lattice[33,34] and the radiation is weak. The rectangular lattice is observed in a small mesa[35] where the surface potential favors the rectangular lattice. Here we investigate the possible synchronization of the Josephson vortices by the in-plane dissipation.

The simulation results are presented in Fig. 5. When the bias current increases, the Josephson vortices evolve toward a rectangular lattice. The rectangular lattice is achieved only by a high bias current, which is difficult to realize experimentally due to the strong self-heating effect. Our simulations are consistent with the analytical results obtained by Koshelev and Aranson,[17] who found that the rectangular lattice can only be stable in a high velocity region. The in-plane dissipation does not stabilize the in-phase plasma oscillation or rectangular lattice of Josephson vortices due to the strong intervortex repulsion. The realization of the in-phase oscillation in the case of Josephson vortices is still an open problem and requires a new mechanism.
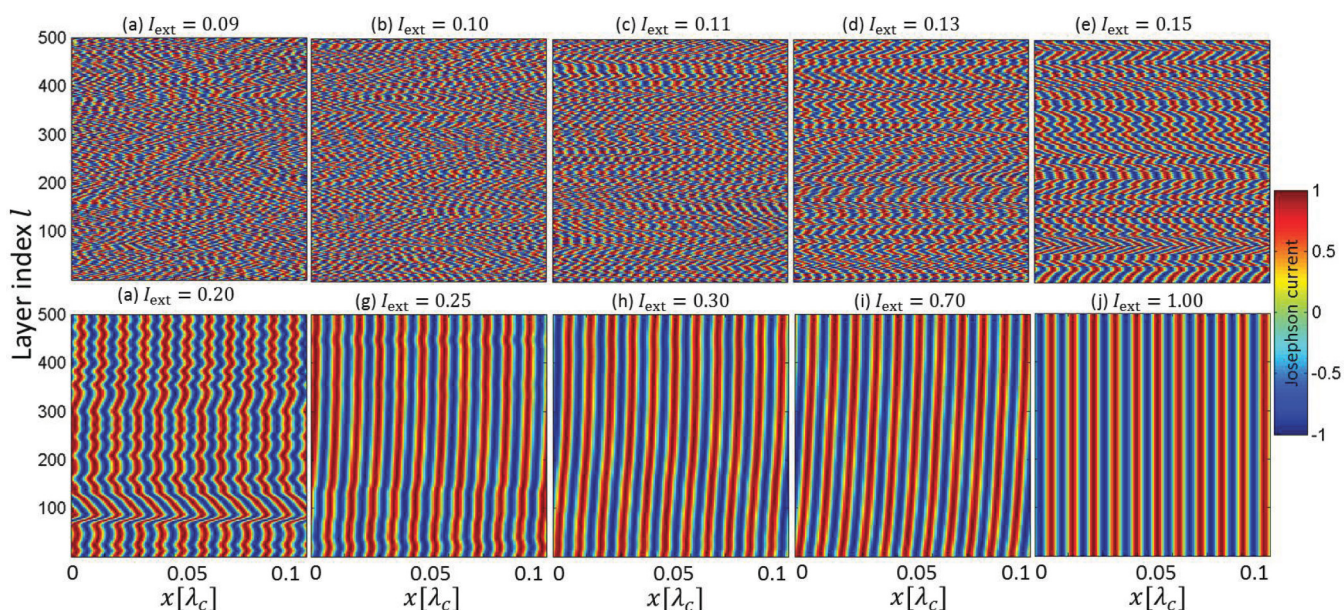
FIG. 5. (Color online) Snapshots of the Josephson current $\sin(\varphi_l)$ in the flux-flow region with the in-plane dissipation $\beta_{ab} = 0.2$. Here the applied magnetic field is $B_a = 1$ T, $L_x = 0.1\lambda_c$, $N = 500$, $\zeta = 7.1 \times 10^4$. The core of Josephson vortex is located at $\varphi = (2m + 1)\pi$.

*szl@lanl.gov

[1] R. Kleiner, F. Steinmeyer, G. Kunkel, and P. Müller, Phys. Rev. Lett. **68**, 2394 (1992).

[2] X. Hu and S. Z. Lin, Supercond. Sci. Technol. **23**, 053001 (2010).

[3] S. Savel'ev, V. A. Yampol'skii, A. L. Rakhmanov, and F. Nori, Rep. Prog. Phys. **73**, 026501 (2010).

[4] L. Ozyuzer, A. E. Koshelev, C. Kurter, N. Gopalsami, Q. Li, M. Tachiki, K. Kadowaki, T. Yamamoto, H. Minami, H. Yamaguchi, T. Tachiki, K. E. Gray, W. K. Kwok, and U. Welp, Science **318**, 1291 (2007).

[5] K. Kadowaki, H. Yamaguchi, K. Kawamata, T. Yamamoto, H. Minami, I. Kakeya, U. Welp, L. Ozyuzer, A. Koshelev, C. Kurter, K. Gray, and W.-K. Kwok, Physica C **468**, 634 (2008).

[6] H. B. Wang, S. Guénon, J. Yuan, A. Iishi, S. Arisawa, T. Hatano, T. Yamashita, D. Koelle, and R. Kleiner, Phys. Rev. Lett. **102**, 017006 (2009).

[7] H. B. Wang, S. Guénon, B. Gross, J. Yuan, Z. G. Jiang, Y. Y. Zhong, M. Gruenzweig, A. Iishi, P. H. Wu, T. Hatano, D. Koelle, and R. Kleiner, Phys. Rev. Lett. **105**, 057002 (2010).

[8] M. Tsujimoto, K. Yamaki, K. Deguchi, T. Yamamoto, T. Kashiwagi, H. Minami, M. Tachiki, K. Kadowaki, and R. A. Klemm, Phys. Rev. Lett. **105**, 037005 (2010).

[9] M. Tsujimoto, T. Yamamoto, K. Delfanazari, R. Nakayama, T. Kitamura, M. Sawamura, T. Kashiwagi, H. Minami, M. Tachiki, K. Kadowaki, and R. A. Klemm, Phys. Rev. Lett. **108**, 107006 (2012).

[10] S. Z. Lin and X. Hu, Phys. Rev. Lett. **100**, 247006 (2008).

[11] A. E. Koshelev, Phys. Rev. B **78**, 174509 (2008).

[12] R. Kleiner, Phys. Rev. B **50**, 6919 (1994).

[13] S. Sakai, P. Bodin, and N. F. Pedersen, J. Appl. Phys. **73**, 2411 (1993).

[14] L. N. Bulaevskii, M. Zamora, D. Baeriswyl, H. Beck, and J. R. Clem, Phys. Rev. B **50**, 12831 (1994).

[15] L. N. Bulaevskii, D. Domínguez, M. P. Maley, A. R. Bishop, and B. I. Ivlev, Phys. Rev. B **53**, 14601 (1996).

[16] M. Machida, T. Koyama, and M. Tachiki, Phys. Rev. Lett. **83**, 4618 (1999).

[17] A. E. Koshelev and I. Aranson, Phys. Rev. B **64**, 174508 (2001).

[18] The inductive coupling is defined as $\zeta = (\lambda_{ab}/s)^2$ and the renormalized conductivities along the c axis and ab plane are defined as $\beta_c = 4\pi\sigma_c/(\epsilon_c\omega_J)$ and $\beta_{ab} = 4\pi\sigma_{ab}\lambda_{ab}^2/(\lambda_c^2\epsilon_c\omega_J)$ with the Josephson

plasma frequency $\omega_J = c/(\lambda_c\sqrt{\epsilon_c})$. Here λ_{ab} and λ_c are the London penetration depths and s is the period of the stack of IJJs. In Eqs. (1) and (2), frequency is in units of ω_J, length is in units of λ_c and magnetic field is in units of $\Phi_0/(2\pi\lambda_c s)$ with $\Phi_0 = hc/(2e)$ the flux quantum. For BSCCO, $\omega_J/(2\pi) \approx 0.1$THz, $\lambda_{ab} \approx 0.4\,\mu$m, and $\lambda_c \approx 200\,\mu$m. The dimensionless electric field is given by $E_{z,l} = \partial_t\varphi_l$, with E in units of $\Phi_0\omega_J/(2\pi cs)$.

[19] S.-F. Lee, D. C. Morgan, R. J. Ormeno, D. M. Broun, R. A. Doyle, J. R. Waldram, and K. Kadowaki, Phys. Rev. Lett. **77**, 735 (1996).

[20] D. B. Romero, C. D. Porter, D. B. Tanner, L. Forro, D. Mandrus, L. Mihaly, G. L. Carr, and G. P. Williams, Phys. Rev. Lett. **68**, 1590 (1992).

[21] Y. I. Latyshev, A. E. Koshelev, and L. N. Bulaevskii, Phys. Rev. B **68**, 134504 (2003).

[22] Y. I. Latyshev, T. Yamashita, L. N. Bulaevskii, M. J. Graf, A. V. Balatsky, and M. P. Maley, Phys. Rev. Lett. **82**, 5345 (1999).

[23] J. Corson, J. Orenstein, S. Oh, J. O'Donnell, and J. N. Eckstein, Phys. Rev. Lett. **85**, 2569 (2000).

[24] L. N. Bulaevskii and A. E. Koshelev, Phys. Rev. Lett. **97**, 267001 (2006).

[25] L. N. Bulaevskii and A. E. Koshelev, Phys. Rev. Lett. **99**, 057002 (2007).

[26] S.-Z. Lin, X. Hu, and L. Bulaevskii, Phys. Rev. B **84**, 104501 (2011).

[27] S. Pagano, M. P. Soerensen, R. D. Parmentier, P. L. Christiansen, O. Skovgaard, J. Mygind, N. F. Pedersen, and M. R. Samuelsen, Phys. Rev. B **33**, 174 (1986).

[28] S. Z. Lin and X. Hu, Phys. Rev. B **79**, 104507 (2009).

[29] S. Z. Lin and X. Hu, Physica C **470**, S201 (2010).

[30] A. E. Koshelev, Phys. Rev. B **82**, 174512 (2010).

[31] V. M. Krasnov, N. Mros, A. Yurgens, and D. Winkler, Phys. Rev. B **59**, 8463 (1999).

[32] M. H. Bae, H. J. Lee, and J. H. Choi, Phys. Rev. Lett. **98**, 027002 (2007).

[33] S. M. Kim, H. B. Wang, T. Hatano, S. Urayama, S. Kawakami, M. Nagao, Y. Takano, T. Yamashita, and K. Lee, Phys. Rev. B **72**, 140504 (2005).

[34] V. M. Krasnov, N. Mros, A. Yurgens, and D. Winkler, Phys. Rev. B **59**, 8463 (1999).

[35] S. O. Katterwe and V. M. Krasnov, Phys. Rev. B **80**, 020502 (2009).